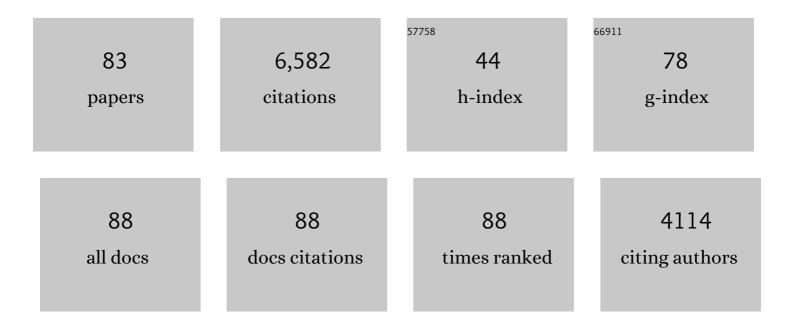
List of Publications by Year in descending order

Source: https://exaly.com/author-pdf/5344758/publications.pdf Version: 2024-02-01



YUDI FIALKO

#	Article	IF	CITATIONS
1	The complete (3-D) surface displacement field in the epicentral area of the 1999MW7.1 Hector Mine Earthquake, California, from space geodetic observations. Geophysical Research Letters, 2001, 28, 3063-3066.	4.0	458
2	Three-dimensional deformation caused by the Bam, Iran, earthquake and the origin of shallow slip deficit. Nature, 2005, 435, 295-299.	27.8	403
3	Coseismic Deformation from the 1999 Mw 7.1 Hector Mine, California, Earthquake as Inferred from InSAR and GPS Observations. Bulletin of the Seismological Society of America, 2002, 92, 1390-1402.	2.3	384
4	Interseismic strain accumulation and the earthquake potential on the southern San Andreas fault system. Nature, 2006, 441, 968-971.	27.8	340
5	Deformation due to a pressurized horizontal circular crack in an elastic half-space, with applications to volcano geodesy. Geophysical Journal International, 2001, 146, 181-190.	2.4	272
6	Seismic and geodetic evidence for extensive, long-lived fault damage zones. Geology, 2009, 37, 315-318.	4.4	222
7	Evidence of fluid-filled upper crust from observations of postseismic deformation due to the 1992Mw7.3 Landers earthquake. Journal of Geophysical Research, 2004, 109, .	3.3	194
8	Probing the mechanical properties of seismically active crust with space geodesy: Study of the coseismic deformation due to the 1992Mw7.3 Landers (southern California) earthquake. Journal of Geophysical Research, 2004, 109, .	3.3	189
9	Postseismic deformation due to the <i>M</i> <sub><i>w</i></sub> 6.0 2004 Parkfield earthquake: Stressâ€driven creep on a fault with spatially variable rateâ€andâ€state friction parameters. Journal of Geophysical Research, 2009, 114, .	3.3	178
10	Deformation on Nearby Faults Induced by the 1999 Hector Mine Earthquake. Science, 2002, 297, 1858-1862.	12.6	171
11	A unified continuum representation of post-seismic relaxation mechanisms: semi-analytic models of afterslip, poroelastic rebound and viscoelastic flow. Geophysical Journal International, 2010, 182, 1124-1140.	2.4	159
12	Shallow slip deficit due to large strike-slip earthquakes in dynamic rupture simulations with elasto-plastic off-fault response. Geophysical Journal International, 2011, 186, 1389-1403.	2.4	131
13	Slip model of the 2015 <i>M</i> <sub><i>w</i></sub> 7.8 Gorkha (Nepal) earthquake from inversions of ALOSâ€2 and GPS data. Geophysical Research Letters, 2015, 42, 7452-7458.	4.0	129
14	Thermal and mechanical aspects of magma emplacement in giant dike swarms. Journal of Geophysical Research, 1999, 104, 23033-23049.	3.3	127
15	Deformation and seismicity in the Coso geothermal area, Inyo County, California: Observations and modeling using satellite radar interferometry. Journal of Geophysical Research, 2000, 105, 21781-21793.	3.3	119
16	Coseismic slip model of the 2008 Wenchuan earthquake derived from joint inversion of interferometric synthetic aperture radar, GPS, and field data. Journal of Geophysical Research, 2010, 115, .	3.3	111
17	Fusion by earthquake fault friction: Stick or slip?. Journal of Geophysical Research, 2005, 110, .	3.3	100
18	Thermodynamics of lateral dike propagation: Implications for crustal accretion at slow spreading mid-ocean ridges. Journal of Geophysical Research, 1998, 103, 2501-2514.	3.3	99

#	Article	IF	CITATIONS
19	Mitigation of atmospheric phase delays in InSAR data, with application to the eastern California shear zone. Journal of Geophysical Research: Solid Earth, 2015, 120, 5952-5963.	3.4	98
20	A Quantitative Assessment of DInSAR Measurements of Interseismic Deformation: The Southern San Andreas Fault Case Study. Pure and Applied Geophysics, 2012, 169, 1463-1482.	1.9	97
21	Ceodetic slip rates in the southern San Andreas Fault system: Effects of elastic heterogeneity and fault geometry. Journal of Geophysical Research: Solid Earth, 2013, 118, 689-697.	3.4	93
22	Observations and Modeling of Coseismic and Postseismic Deformation Due To the 2015 <i>M<sub>w</sub></i> 7.8 Gorkha (Nepal) Earthquake. Journal of Geophysical Research: Solid Earth, 2018, 123, 761-779.	3.4	92
23	Interseismic deformation and creep along the central section of the North Anatolian Fault (Turkey): InSAR observations and implications for rateâ€andâ€state friction properties. Journal of Geophysical Research: Solid Earth, 2013, 118, 316-331.	3.4	85
24	Localized and distributed creep along the southern San Andreas Fault. Journal of Geophysical Research: Solid Earth, 2014, 119, 7909-7922.	3.4	82
25	Space geodetic investigation of the coseismic and postseismic deformation due to the 2003 <i>M</i> <sub><i>w</i></sub> 7.2 Altai earthquake: Implications for the local lithospheric rheology. Journal of Geophysical Research, 2008, 113, .	3.3	81
26	Sombrero Uplift Above the Altiplano-Puna Magma Body: Evidence of a Ballooning Mid-Crustal Diapir. Science, 2012, 338, 250-252.	12.6	78
27	Finite source modelling of magmatic unrest in Socorro, NewÂMexico, and Long Valley, California. Geophysical Journal International, 2001, 146, 191-200.	2.4	77
28	The 1999 (Mw 7.1) Hector Mine, California, Earthquake: Near-Field Postseismic Deformation from ERS Interferometry. Bulletin of the Seismological Society of America, 2002, 92, 1433-1442.	2.3	73
29	Fourier-domain Green's function for an elastic semi-infinite solid under gravity, with applications to earthquake and volcano deformation. Geophysical Journal International, 0, 182, 568-582.	2.4	71
30	Upper-plate controls on co-seismic slip in the 2011 magnitude 9.0 Tohoku-oki earthquake. Nature, 2016, 531, 92-96.	27.8	69
31	Warping and cracking of the Pacific plate by thermal contraction. Journal of Geophysical Research, 2004, 109, .	3.3	68
32	Slip on faults in the Imperial Valley triggered by the 4 April 2010 Mw 7.2 El Mayor-Cucapah earthquake revealed by InSAR. Geophysical Research Letters, 2011, 38, n/a-n/a.	4.0	68
33	Evidence for on-going inflation of the Socorro Magma Body, New Mexico, from interferometric synthetic aperture radar imaging. Geophysical Research Letters, 2001, 28, 3549-3552.	4.0	67
34	â€~Melt welt' mechanism of extreme weakening of gabbro at seismic slip rates. Nature, 2012, 488, 638-641.	27.8	67
35	El Mayor-Cucapah ( <i>M<sub>w</sub></i> 7.2) earthquake: Early near-field postseismic deformation from InSAR and GPS observations. Journal of Geophysical Research: Solid Earth, 2014, 119, 1482-1497.	3.4	66
36	Dynamic models of interseismic deformation and stress transfer from plate motion to continental transform faults. Journal of Geophysical Research, 2012, 117, .	3.3	58

#	Article	IF	CITATIONS
37	Finite Slip Models of the 2019 Ridgecrest Earthquake Sequence Constrained by Space Geodetic Data and Aftershock Locations. Bulletin of the Seismological Society of America, 2020, 110, 1660-1679.	2.3	56
38	Coseismic and Early Postseismic Deformation Due to the 2021 M7.4 Maduo (China) Earthquake. Geophysical Research Letters, 2021, 48, e2021GL095213.	4.0	56
39	Interseismic Strain Localization in the San Jacinto Fault Zone. Pure and Applied Geophysics, 2014, 171, 2937-2954.	1.9	54
40	Temperature fields generated by the elastodynamic propagation of shear cracks in the Earth. Journal of Geophysical Research, 2004, 109, .	3.3	51
41	Three-dimensional models of elastostatic deformation in heterogeneous media, with applications to the Eastern California Shear Zone. Geophysical Journal International, 2009, 179, 500-520.	2.4	50
42	Stable and unstable damage evolution in rocks with implications to fracturing of granite. Geophysical Journal International, 2006, 167, 1005-1016.	2.4	49
43	A silent <i>M</i> <sub><i>w</i></sub> 4.7 slip event of October 2006 on the Superstition Hills fault, southern California. Journal of Geophysical Research, 2009, 114, .	3.3	49
44	Structure and mechanical properties of faults in the North Anatolian Fault system from InSAR observations of coseismic deformation due to the 1999 Izmit (Turkey) earthquake. Journal of Geophysical Research, 2007, 112, .	3.3	47
45	Temperature dependence of frictional healing of Westerly granite: Experimental observations and numerical simulations. Geochemistry, Geophysics, Geosystems, 2013, 14, 567-582.	2.5	46
46	Slow Slip Event On the Southern San Andreas Fault Triggered by the 2017 <i>M</i> <sub><i>w</i></sub> 8.2 Chiapas (Mexico) Earthquake. Journal of Geophysical Research: Solid Earth, 2019, 124, 9956-9975.	3.4	46
47	On origin of near-axis volcanism and faulting at fast spreading mid-ocean ridges. Earth and Planetary Science Letters, 2001, 190, 31-39.	4.4	45
48	Effect of a compliant fault zone on the inferred earthquake slip distribution. Journal of Geophysical Research, 2008, 113, .	3.3	44
49	The Community Code Verification Exercise for Simulating Sequences of Earthquakes and Aseismic Slip (SEAS). Seismological Research Letters, 2020, 91, 874-890.	1.9	43
50	Estimate of differential stress in the upper crust from variations in topography and strike along the San Andreas fault. Geophysical Journal International, 2005, 160, 527-532.	2.4	41
51	Frictional properties of gabbro at conditions corresponding to slow slip events in subduction zones. Geochemistry, Geophysics, Geosystems, 2015, 16, 4006-4020.	2.5	41
52	Fracture criteria at the tip of fluid-driven cracks in the Earth. Geophysical Research Letters, 1995, 22, 2541-2544.	4.0	39
53	Space geodetic observations and models of postseismic deformation due to the 2005 <i>M </i> 7.6 Kashmir (Pakistan) earthquake. Journal of Geophysical Research: Solid Earth, 2014, 119, 7306-7318.	3.4	38
54	Numerical simulation of high-pressure rock tensile fracture experiments: Evidence of an increase in fracture energy with pressure?. Journal of Geophysical Research, 1997, 102, 5231-5242.	3.3	36

#	Article	IF	CITATIONS
55	Hydrologic detection and finite element modeling of a slow slip event in the Costa Rica prism toe. Journal of Geophysical Research, 2009, 114, .	3.3	36
56	A comparison of longâ€ŧerm changes in seismicity at The Geysers, Salton Sea, and Coso geothermal fields. Journal of Geophysical Research: Solid Earth, 2016, 121, 225-247.	3.4	36
57	Mechanics of active magmatic intraplating in the Rio Grande Rift near Socorro, New Mexico. Journal of Geophysical Research, 2010, 115, .	3.3	35
58	Velocityâ€weakening behavior of Westerly granite at temperature up to 600°C. Journal of Geophysical Research: Solid Earth, 2016, 121, 6932-6946.	3.4	34
59	What controls the along-strike slopes of volcanic rift zones?. Journal of Geophysical Research, 1999, 104, 20007-20020.	3.3	33
60	On the effects of thermally weakened ductile shear zones on postseismic deformation. Journal of Geophysical Research: Solid Earth, 2013, 118, 6295-6310.	3.4	33
61	Geodetic constraints on frictional properties and earthquake hazard in the Imperial Valley, Southern California. Journal of Geophysical Research: Solid Earth, 2016, 121, 1097-1113.	3.4	32
62	Rising of the lowest place on Earth due to Dead Sea waterâ€level drop: Evidence from SAR interferometry and GPS. Journal of Geophysical Research, 2012, 117, .	3.3	31
63	Geodetic investigation into the deformation of the Salton Trough. Journal of Geophysical Research: Solid Earth, 2013, 118, 5030-5039.	3.4	31
64	Experimental investigation of frictional melting of argillite at high slip rates: Implications for seismic slip in subductionâ€accretion complexes. Journal of Geophysical Research, 2009, 114, .	3.3	27
65	Improving Burst Alignment in TOPS Interferometry With Bivariate Enhanced Spectral Diversity. IEEE Geoscience and Remote Sensing Letters, 2017, 14, 2423-2427.	3.1	22
66	Simple shear origin of the cross-faults ruptured in the 2019 Ridgecrest earthquake sequence. Nature Geoscience, 2021, 14, 513-518.	12.9	22
67	Reconciling seismicity and geodetic locking depths on the Anza section of the San Jacinto fault. Geophysical Research Letters, 2016, 43, 10,663.	4.0	21
68	Why do kimberlites from different provinces have similar trace element patterns?. Geochemistry, Geophysics, Geosystems, 2005, 6, n/a-n/a.	2.5	18
69	Variations in the long-term uplift rate due to the Altiplano–Puna magma body observed with Sentinel-1 interferometry. Earth and Planetary Science Letters, 2018, 491, 43-47.	4.4	18
70	Estimation of Absolute Stress in the Hypocentral Region of the 2019 Ridgecrest, California, Earthquakes. Journal of Geophysical Research: Solid Earth, 2021, 126, e2021JB022000.	3.4	18
71	Geodetic Evidence for a Blind Fault Segment at the Southern End of the San Jacinto Fault Zone. Journal of Geophysical Research: Solid Earth, 2018, 123, 878-891.	3.4	17
72	Survey and Continuous GNSS in the Vicinity of the July 2019 Ridgecrest Earthquakes. Seismological Research Letters, 2020, 91, 2047-2054.	1.9	17

#	Article	IF	CITATIONS
73	Subsidence at Cerro Prieto Geothermal Field and postseismic slip along the Indiviso fault from 2011 to 2016 RADARSATâ€2 DInSAR time series analysis. Geophysical Research Letters, 2017, 44, 2716-2724.	4.0	16
74	Can compliant fault zones be used to measure absolute stresses in the upper crust?. Journal of Geophysical Research, 2009, 114, .	3.3	14
75	Fracture and Frictional Mechanics: Theory. , 2015, , 73-91.		12
76	Tidal modulation of seismicity at the Coso geothermal field. Earth and Planetary Science Letters, 2022, 579, 117335.	4.4	11
77	Obtaining Absolute Locations for Quarry Seismicity Using Remote Sensing Data. Bulletin of the Seismological Society of America, 2006, 96, 722-728.	2.3	10
78	Fracture and Frictional Mechanics $\hat{a} \in$ "Theory. , 2007, , 83-106.		8
79	Lithospheric Deformation Due To the 2015 M7.2 Sarez (Pamir) Earthquake Constrained by 5Âyears of Space Geodetic Observations. Journal of Geophysical Research: Solid Earth, 2022, 127, .	3.4	7
80	General Seismic Architecture of the Southern San Andreas Fault Zone around the Thousand Palms Oasis from a Large-N Nodal Array. The Seismic Record, 2022, 2, 50-58.	3.1	6
81	Fracture and Frictional Mechanics – Theory. , 2007, , 83-106.		3
82	Comment on "Deformation of compliant fault zones induced by nearby earthquakes: Theoretical investigations in two dimensions―by Benchun Duan et al Journal of Geophysical Research, 2011, 116, .	3.3	2
83	Damage rheology and stable versus unstable fracturing of rocks. , 2009, , 133-144.		0